Applied Catalysis B: Environmental 193 (2016) 121–132

Contents lists available at ScienceDirect

Applied Catalysis B: Environmental

journal homepage: www.elsevier.com/locate/apcatb

Kinetics of Hg° oxidation over a $V_2O_5/MoO_3/TiO_2$ catalyst: Experimental and modelling study under $DeNO_X$ inactive conditions

Nicola Usberti [a], Silvia Alcove Clave [b], Michael Nash [b], Alessandra Beretta [a,*]

[a] Dipartimento di Energia, Politecnico di Milano, via La Masa 34, 20156 Milano, Italy
[b] Johnson Matthey, Technology Center, Sonning Common, RG4 9NH, United Kingdom

ARTICLE INFO

Article history:
Received 14 January 2016
Received in revised form 24 March 2016
Accepted 30 March 2016
Available online 1 April 2016

Keywords:
Hg oxidation
SCR catalyst
Effect of HCl
Kinetic study
Reactor model

ABSTRACT

In this work, a kinetic study of mercury oxidation over a commercial plate-type V/Mo/Ti/O catalyst was addressed by investigating the effects of key operating variables (temperature, HCl and Hg° concentration). The study was performed under reference $DeNO_X$-inactive conditions, that is in the absence of NO_X, NH_3, SO_X, recognizing that surface coverage effects can greatly affect the kinetics of this complex reacting system. Aim of the work was in fact to better clarify the nature of the intrinsic reaction (in particular its temperature dependence), that, despite the increasing interest toward this reaction, is still debated with a very large scatter among observations. The experiments were performed over slabs. The combined effects of temperature and HCl concentration evidenced that the conversion of Hg° was independent from the HCl content below 300–325 °C, where the reaction showed a positive temperature dependence; at higher temperature, the conversion of Hg° became highly sensitive to the HCl concentration, which determined the observed temperature dependence (negative at 2.5 ppm HCl, positive at 50 ppm HCl). Thus the data suggest a strong dependence of the reaction kinetics on the surface coverage of HCl.

A model of the reactor cell was developed and an engineering analysis of data was performed to decouple the effects of inter-phase and intra-porous mass transfer limitations. A rate expression was derived from the formalization of a redox reaction scheme wherein a step-wise oxy-chlorination process ($Hg^\circ \rightarrow HgCl_{ads} \rightarrow HgCl_2$) is assumed in line with recent theoretical findings. By assuming that the surface coverages of the HgCl intermediate and the reduced sites are negligible with respect to the coverage of free and chlorinated oxidized sites, a simple rate expression is derived which accounts for a quadratic dependence on HCl coverage and a linear dependence on the gas-phase concentration of elemental mercury (in line with the experimental evidence). The whole bulk of data could be well described, capturing the key observed trends. The activation energy of the reaction steps was found to be 14000 cal/mole while the enthalpy of HCl activation was estimated at −20000 cal/mole, coherently with the energetics of V-sites chlorination.

1. Introduction

Coal-fired power plants, waste incinerators, and cements plants are the major anthropogenic sources of mercury emission; due to its persistence, long-range mobility in air, bio-accumulation in water, and neuro-toxic impact on human health, mercury is regarded as a hazardous atmospheric pollutant and its abatement represents a new challenge for environmental catalysis [1–4].

The technology implemented for the control of mercury emissions from stationary applications and their effectiveness are strongly related to the nature of mercury species in the flue gases. While oxidized mercury (Hg^{2+}) and particle-bound mercury (Hg^P) are easy to remove using typical APCDs, elemental mercury (Hg°) is difficult to capture due to its high volatility and low solubility in water [5–7]. Among all the technologies, catalytic oxidation of elemental mercury to ionic mercury, combined with ESP/FF and/or wet scrubbing, is presently the most promising method to achieve, in a cost effective way, such a target [1]. Consequently, one of the main objectives of mercury emission control strategies in power plants is the efficient conversion of elemental mercury into oxidized mercury.

It is now well known in the literature that the highly desired conversion of Hg° to Hg^{2+} can be achieved as a co-benefit of the

* Corresponding author.
E-mail address: alessandra.beretta@polimi.it (A. Beretta).

http://dx.doi.org/10.1016/j.apcatb.2016.03.071
0926-3373/

presence of a SCR-DeNO$_X$ unit [8,9]. In the presence of HCl, SCR catalysts affect mercury speciation according to the stoichiometry:

$$Hg + 2HCl + 1/2O_2 \rightarrow HgCl_2 + H_2O \quad (1)$$

V_2O_5-WO_3(MoO_3)/TiO_2 catalysts are well established SCR catalysts and their activity in reaction (1) has been largely documented; both lab-scale tests (Kamata et al. [8]) and pilot scale tests (Beretta et al. [10]) have shown for instance a systematic increase of Hg° oxidation efficiency with increasing V content of the catalyst.

Although mercury oxidation over V_2O_5-based catalysts has been deeply investigated, the mechanism and kinetics of this reaction are still under investigation. So far, a number of macroscopic kinetic effects have been unanimously recognized in the scientific and technical literature. For instance the presence of HCl is reported to be the most effective component responsible for Hg° oxidation since the major oxidized mercury species in coal-derived flue gas is $HgCl_2$. Also, it has been reported that the rate of Hg° oxidation is negligible in the absence of HCl, in which case adsorption and surface accumulation of mercury-species occurs [11,12]. Several authors have shown that the promoting effect of the HCl concentration has an asymptotic trend on mercury oxidation activity when explored in a wide concentration range [8,13–16].

However, there is disagreement regarding the specific interactions between Hg, HCl, and the catalyst surface. Vosteen et al. [17] first suggested that Hg oxidation proceeds via the Deacon process, so that HCl is oxidized by the V_2O_5/TiO_2 catalyst to form Cl_2, and then Cl_2 promotes Hg oxidation via a gas phase reaction. On the other hand, tests performed by He et al. [18] and a modeling study carried out by Niksa and Fujiwara [19] demonstrated that gas-phase reactions cannot account for the extent of mercury oxidation. Eom et al. [20] proposed that Hg oxidation occurs with reactive Cl-species, generated from adsorbed HCl, reacting with an adjacent adsorbed Hg° according to a Langmuir-Hinshelwood mechanism. Senior [21] suggested instead an Eley-Rideal reaction mechanism, in which elemental mercury adsorbs on the catalyst surface and then reacts with gas phase HCl. Recently, Zhang et al. [22] claimed that mercury oxidation occurs through an Eley-Rideal mechanism that involves the reaction between gas phase elemental mercury and HCl adsorbed and dissociated on V_2O_5 sites. Therefore, a full agreement on the reaction mechanism of Hg oxidation over V-based catalysts is still missing. Recent theoretical studies, though, support the hypothesis that the reaction involves both the activation of HCl with the formation of an oxy-chlorinated V-site, and the interaction (although weak) of Hg with a V = O site [23].

The complexity of the process emerges from the broad scatter of the experimental evidence. For instance there is no unanimous identification of the temperature dependence of the process. Yang et al. [24] performed dedicated tests over V_2O_5–WO_3/TiO_2 powders in the presence of HCl and oxygen without co-feeding SCR reactants: an increasing trend of Hg° oxidation vs temperature was found in the range between 200 °C to 350 °C. A similar trend was observed by Negreira and Wilcox [25], with an estimation of the apparent activation energy of about 8.5 kcal/mol. Conversely, under typical NH_3-SCR conditions (with the presence of both NO and NH_3 in the inlet mixture), the effect of temperature on mercury oxidation has been reported to be moderate or even negative [1].

These widely varying results may be associated with the large number of factors which expectedly influence the experiment. On one side, it has been shown that the process is affected by external mass transfer limitations, in analogy with the case of the SCR reaction [19], which can explain low values of the apparent activation energy when the experiments are performed over plates or monoliths. On the other side, Madsen et al. [26,27] have recently shown, by running experiments over a proprietary V-based catalyst at low space velocity and comparing them with thermochemical equilibrium calculations, that the oxy-chlorination of Hg° (Eq. (1)) is a reversible process and the thermodynamics are such that Hg° is the favored species at high temperatures. Indeed, the impact of thermodynamics on the speciation of mercury is well known in the literature of gas-phase chemistry in incinerators and burners [28–30]. Thus, a moderate or even negative temperature dependence of Hg° conversion could be associated with the approach to thermodynamic equilibrium, especially if the experiments are run at very high temperatures and low HCl concentrations.

In addition, the efficiency of the Hg° oxidation reaction is deeply affected by the flue gas composition, particularly by the co-presence of DeNO$_X$ reactants (NH_3 and NO). It is widely recognized that Hg° oxidation is inhibited by NH_3 [9,12,13,16,31–33]: this was usually explained invoking a competitive adsorption of ammonia on the active vanadium sites. Recently, Madsen et al. [26,27] have better shown that the NH_3 apparently acts as a reducing agent for $HgCl_2$, at temperatures higher than 325 °C according to the reaction:

$$HgCl_2 + 2/3NH_3 \rightarrow Hg + 1/3N_2 + 2HCl \quad (2)$$

This assumption was experimentally confirmed by Koeser et al. [16] from combined DeNO$_X$ and Hg-oxidation tests over SCR monoliths: the results showed that ammonia can effectively reduce $HgCl_2$ to elemental mercury at 390 °C. This effect could explain the negative temperature trend typically observed in the range of temperatures between 300 °C and 400 °C in the presence of NH_3 co-feed.

Finally, Madsen et al. [26,27] reported that the co-presence of both NO$_X$ and NH_3 (the so-called "NH_3-DeNO$_X$ active" conditions) decreased the rate of mercury oxidation, which was associated to the partial "occupation" of redox sites by the DeNO$_X$ process; in other terms, the authors propose that the DeNO$_X$ process and the Hg° oxidation process share the same redox V-sites.In this work we addressed a kinetic study of Hg° oxy-chlorination on a JM proprietary catalyst, aiming at the identification of the prevailing kinetic dependences and their quantitative interpretation in the form of a kinetic scheme. Based on the general understanding that the chemical process is strongly influenced by the interaction with chemical species which may interact with the catalyst surface, on purpose we first addressed a study under reference "DeNO$_X$ inactive" conditions (absence of NO and NH_3 in the reacting mixture). In the present paper, thus, we address the experimental and modelling analysis of the effects of fundamental parameters, reaction temperature and HCl concentration, trying to characterize the temperature dependence of the reaction and the kinetic role of HCl. The pursued aim is in fact a better comprehension of the intrinsic process kinetics, which in turn can help towards the identification of the rate determining step and the nature of surface intermediates, and, in perspective, provide guidelines for improving the catalyst formulations.

2. Experimental

SCR and Hg° oxidation experiments were performed over a Johnson Matthey V_2O_5/MoO_3/TiO_2 catalyst developed for High-Dust applications in coal-fired power plants. It is a plate-type catalyst, cut in slabs for the lab-scale testing, with a medium-low V_2O_5 content.

A diagram of the testing unit is reported in Fig. 1.

All the flue gases components are supplied by gas cylinders (compositions: pure N_2, pure O_2, 10% NO in N_2; 10% NH_3 in N_2; 5% HCl in N_2) and their flow rates are controlled by mass flow controllers. Water is introduced by a peristaltic pump and evaporated in a boiler. Elemental mercury (Hg°) vapor is provided by flowing nitrogen through a saturated mercury source (Tekran instrument 3310) kept at constant temperature: the mercury concentration in

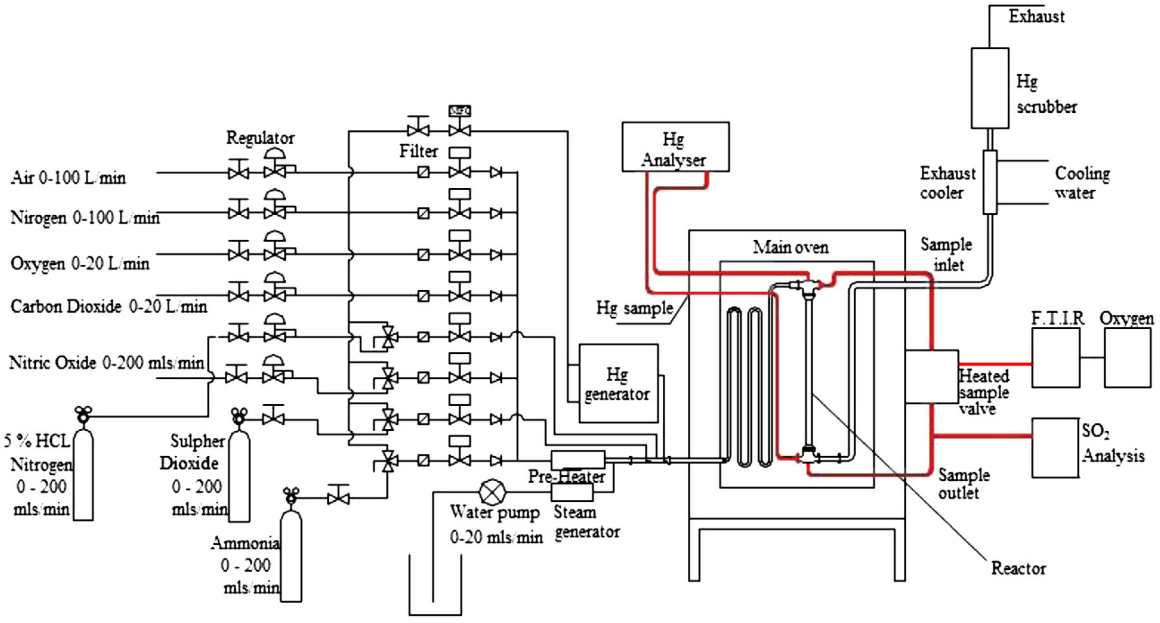

Fig. 1. Flow diagram of the experimental setup.

the simulated flue gas can be adjusted by varying the temperature of the mercury source and the flow rate of nitrogen. All components, with the exception of HCl and Hg, are first mixed together in a preheater, placed outside the main oven at around 180 °C, and then delivered to a serpentine tube placed in the furnace upstream from the reactor. HCl and Hg are, instead, inserted through separated lines and mixed inside the oven in order to avoid low temperature reactions. In the oven, all the lines and connections were made of quartz, in order to avoid corrosion phenomena due to the presence of acid compounds in the fed mixture.

The reactor consisted of a rectangular quartz tube (internal cross-section 32 × 28 mm), wherein two sample holders allowed for the placement of four slabs (400 mm long) in a parallel configuration. Thus, the reaction cell cross section was divided in 5 rectangular channels. A furnace was used to heat the reactor cell at the desired temperature.

A bypass system allowed the online measurement of NO_X, NH_3, and HCl concentration both upstream and downstream of the reactor using a Midac FTIR analyzer; O_2 content was evaluated by means of a paramagnetic analyzer.

The mercury concentration measurements were performed using a dedicated apparatus (Tekran instrument): the flue gas sampled by the instrument was split into two streams. In the first stream, a thermal conditioner unit converted all mercury species into Hg° (allowing the analyzer to measure the total mercury present in the gas flow) while the second pathway removed oxidized mercury (water soluble) with a scrubber, in order to measure only the elemental mercury concentration. Alternatively, one of these streams was pulled through a cartridge containing ultra-pure gold adsorbent, where the mercury was collected. The mercury was then thermally desorbed in an argon gas stream and detected by an integrated cold vapor atomic fluorescence spectrometer (CVAFS). The instrument operated these two cartridges in parallel, with alternating operation modes (sampling and desorbing/analyzing) on a time base of 5 min. The accuracy of the Tekran mercury analyzer is guaranteed by a daily calibration procedure, which consists of injecting a gas stream with known Hg° concentration provided by a Tekran 3310 unit. The gas stream was injected just after the sample switch point. The 3310 units are calibrated according to a NIST standard [34]. Furthermore, this system was able to automatically switch the sampling spot from upstream to downstream of the reactor using special connections, thus measuring in a continuous mode the total mercury and the elemental mercury concentrations at the inlet (respectively called Hg_{IN}^{TOT}, Hg_{IN}^{0}) and at the outlet of the reactor (Hg_{OUt}^{TOT}, Hg_{OUt}^{0}). Fig. 2, panel a, shows an example of raw experimental data provided by the mercury analyzer over time during Hg oxidation reference tests.

The measurements of the total mercury concentration and the elemental mercury concentration were used to evaluate Hg° conversion across and before the reactor and the total Hg balance, according to the following expressions:

$$Hg^{TOT}\,Balance\,[\%] = \frac{Hg_{IN}^{TOT} - \left(Hg_{IN}^{TOT} - Hg_{OUT}^{TOT}\right)}{Hg_{IN}^{TOT}} \times 100; \quad (3)$$

$$Hg^{0}\,Conversion\,before\,reactor\,[\%] = \frac{Hg_{IN}^{TOT} - Hg_{IN}^{0}}{Hg_{IN}^{TOT}} \times 100; \quad (4)$$

$$Hg^{0}\,Conversion\,[\%] = \frac{Hg_{IN}^{0} - Hg_{OUT}^{0}}{Hg_{IN}^{0}} \times 100. \quad (5)$$

Fig. 2b exemplifies the trend over time of the parameters calculated with Eqs. (3)–(5) from the raw data of Fig. 2a.

Hg^{TOT}balance was calculated with Eq. (3) as the difference between the total mercury upstream (Hg_{IN}^{TOT}) and downstream (Hg_{OUT}^{TOT}) of the reactor: its value was lower than 100% in the whole set of experiments performed and its complement represents the amount of the mercury that is possibly captured on the catalyst or lost during transport to the analyzer. Mercury oxidation tests showed that a small amount of oxidized mercury was always detected at the inlet of the reactor, probably due to homogeneous reactions or interaction between elementary mercury and the impurities deposited on the rig's lines upstream of the catalyst bed. This effect can be quantified as shown by Eq. (4), by analyzing the total mercury (Hg_{IN}^{TOT}) and the elemental mercury (Hg_{IN}^{0}) detected in correspondence to the inlet of the reactor. Fig. 2-panel b shows that mercury conversion before the reactor was limited but not negligible and amounted to 5–10% of the total mercury fed. Finally, the measure of mercury speciation at the outlet of the reactor allowed to evaluate the conversion of elemental mercury, as described by Eq. (5), based on the comparison between

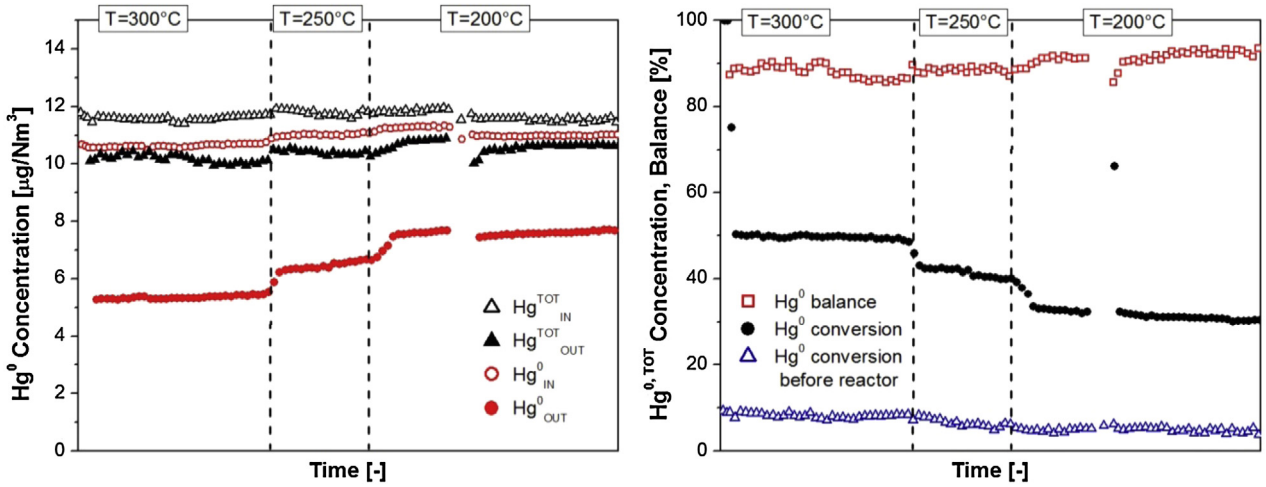

Fig. 2. Left panel: Hg oxidation tests, measured total mercury and elemental mercury at the inlet and at the outlet of the reactor over time. Right panel: Hg oxidation tests, calculated total mercury balance, elemental mercury conversion and elemental mercury conversion before the reactor over time. Operating conditions: T = 300-250-200 °C. Feed composition: Hg° = 10 μg/Nm³; HCl = 10 ppm; H_2O = 10.5%; O_2 = 3.5%; N_2 at balance. AV = 21 Nm/h.

the concentration of elemental mercury at the reactor inlet (Hg^0_{IN}) and the concentration of elemental mercury at the reactor outlet (Hg^0_{OUT}). The conversion of elemental mercury, though not necessarily representative of the conversion to oxidized mercury, is the most commonly adopted quantity to express the process efficiency [19].

Steady-state experimental data were collected when stationary Hg° conversion performances were reached. Furthermore, experimental data characterized by Hg° balance lower than 80% or Hg° conversion before the reactor higher than 20% were discarded.

The experiments were performed under atmospheric pressure at the temperatures of 170–400 °C. The total gas flow rate passing through the reactor was kept at 28 Nl/min, corresponding to an area velocity (AV) of 21 Nm/h according to standard temperature and pressure. Mercury oxidation tests were performed feeding an inlet mixture of 10 μg/Nm³ Hg°, 3.5% O_2, 10.5% H_2O and N_2 as carrier gas, varying the composition of HCl (0–50 ppm). Experiments under central operating conditions (300 °C, 10 ppm HCl, 10 μg/Nm³ Hg°) were periodically repeated to verify the catalyst stability; throughout the whole experimental campaign no systematic deactivation was observed, since the measured deviations were scattered and always within the experimental uncertainty.

$DeNO_X$ tests were also carried out in the same flow rate conditions by feeding 300 ppm NO, 405 ppm NH_3, 3.5% O_2, 10.5% H_2O and N_2 as carrier gas. Such tests served as a benchmark of the catalyst activity and of the model response.

3. Results and discussion

3.1. Reactor model

A heterogeneous 1D reactor model was applied to analyze quantitatively the data and extract intrinsic kinetics from the tests performed over the slabs. At this scope, the model incorporates a lumped description of both external and internal mass transfer limitations in the channels, each of which was treated as a single Plug Flow Reactor.

Since the size and cross section of the five channels is the same, it was assumed that the total flow rate is equally split among them.

However, we accounted for the fact that inner and outer channels differ for the number of catalytic faces (two catalytic faces for the inner channels, one catalytic face for the lateral channels). The ratio between active (catalytic) perimeter and total wetted perimeter of the channel influences both the rate of mass transfer and the contribution from the reaction at the wall. In this work, we adopted the same approach as in Beretta et al. ([35]) where the performance of plate-type monolithic catalysts for SCR applications was studied; similarly to the present study, also in that study experiments were performed in a multichannel reactor cell and a model was developed which accounted for the difference between inner and outer channels.

Briefly, interphase mass-transfer coefficients for NO, NH_3 and Hg° were estimated by treating the process of gas-phase diffusion and reaction at the wall inside the test-reactor in analogy with the Graetz-Nusselt problem of heat transfer in a rectangular duct with developing laminar flow and constant wall temperature (T condition in Shah and London, 1978). We recall that the adequacy of the analogy between mass and thermal problems has been verified by Tronconi and Forzatti ([36]) for a number of channel shapes in SCR honeycomb monoliths.

The following axial profile of the local Sherwood number was assumed:

$$Sh(z^*) = Sh_\infty + 8.827(1000z^*)^{-0.545}\exp(-48.2z^*) \quad (6)$$

where z^* is the Graetz coordinate and Sh_∞ is the asymptotic value of the Sherwood number. This assumption was successfully applied by Tronconi and Forzatti [36] and Groppi et al. [37] to different channel geometries. The estimates of the asymptotic value of the Sherwood number Sh_∞ depend on both the geometry of the channel and the number and relative position of the active walls. In particular, the internal channel of the test reactor corresponds, in the thermal problem, to a rectangular duct with two opposite adiabatic walls (non-catalytic sides); each lateral channel, instead, may be associated with a rectangular duct with three adiabatic walls. For both these cases, Shah and London list the values of Sh_∞ for rectangular channels at different values of the aspect ratio (smaller size/larger size of the cross section): considering the geometry of the channels involved, we obtained Sh_∞ values of 5.57 and 3.78 respectively for internal and lateral channels. Notably, mass transfer in the central channels is faster than that in the external channels, as a consequence of the shorter diffusion path.

The description of the diffusion process inside the catalytic walls was obtained by adopting the Random Pore Model developed by Wakao and Smith [38] which describes the catalyst wall as an aggregate of microporous particles with interstices, representing the macroposity, and the diffusion flow within the catalyst wall

Table 1
Model equations for simulating the $DeNO_X$ process in each channel.

NO and NH_3 gas-phase mass balances:
$\frac{d\Gamma_{NO}}{dz^*} = -4Sh_{NO}\left(\Gamma_{NO}^{bulk} - \Gamma_{NO}^{wall}\right)$ (8)
initial condition: $\Gamma_{NO}|_{z^*=0} = 1$ (9)
$\frac{d\Gamma_{NH_3}}{dz^*} = -4Sh_{NH_3}\frac{D_{NH_3}}{D_{NO}}\left(\Gamma_{NH_3}^{bulk} - \Gamma_{NH_3}^{wall}\right)$ (10)
initial condition: $\Gamma_{NH_3}|_{z^*=0} = \alpha$ (11)
with:
$\Gamma_i = C_i/C_{NO}^{IN}$ (12)
NO and NH_3 gas-solid continuity equations:
$Sh_{NO}\left(1\Gamma_{NO}^{bulk} - \Gamma_{NO}^{wall}\right) = \eta Da_{DeNOx}\Gamma_{NO}^{wall}\frac{P_{active}}{P_{wetted}}$ (13)
$Sh_{NO}\left(\Gamma_{NO}^{bulk} - \Gamma_{NO}^{wall}\right) = Sh_{NH_3}\frac{D_{NH_3}}{D_{NO}}\left(\Gamma_{NH_3}^{bulk} - \Gamma_{NH_3}^{wall}\right)$ (14)
with
$\eta = \frac{tanh(\Phi_{DeNOx})}{\Phi_{DeNOx}}$ (15)
$Da_{DeNOx} = k_{DeNOx}d_h h/D_{NO}$ (16)
k_{DeNOx} = kinetic constant for DeNOx process (s^{-1})
h = half thickness of the catalytic slab (cm)
d_h = hydraulic diameter of the channel (cm)
$P_{active,i}$ = *active perimeter of the i^{th} channel (different from internal to lateral channels)*
P_{wetted} = *wetted perimeter of the i^{th} channel (equal from internal to lateral channels)*
Φ_{DeNO_X} = Thiele modulus = $h\sqrt{\frac{k_{DeNOx}}{D_{eff,NO}}}$
z^* = Graetz coordinate = $\frac{z/h}{ReSc}$
z = axial coordinate (cm)

Table 2
Model equations for simulating Hg° oxidation in each channel.

Hg° gas-phase mass balance:
$\frac{d\Gamma_{Hg}}{dz^*} = -4Sh_{Hg}\frac{D_{Hg}}{D_{NO}}\left(\Gamma_{Hg}^{bulk} - \Gamma_{Hg}^{wall}\right)$ (17)
initial condition: $\Gamma_{Hg}|_{z^*=0} = 1$ (18)
with:
$\Gamma_{Hg} = C_{Hg}/C_{Hg}^{IN}$ (19)

Hg° gas-solid continuity equation:
$Sh_{Hg}\left(\Gamma_{Hg}^{bulk} - \Gamma_{Hg}^{wall}\right) = \eta_{Hg}Da_{Hg}R_{Hg}^*\frac{P_{active}}{P_{wetted}}$ (20)
with:
$Da_{Hg} = k_{Hg}d_h h/D_{Hg}$ (21)
$\eta_{Hg} = \frac{\tanh(\Phi_{Hg})}{\Phi_{Hg}}$ (22)
$\Phi_{Hg} = h\sqrt{\frac{k_{Hg}R_{Hg}^*}{\Gamma_{Hg}^{wall}D_{eff,Hg}}}$ (23)
k_{Hg} = intrinsic kinetic constant of Hg° oxidation (s^{-1})

as a combination of molecular and Knudsen diffusion through (i) microporous particles, (ii) macropores and (iii) macro/micro pores in series. At this scope, the morphology of the catalyst coating was characterized by means of N_2-adsorption-desorption analyses and Hg-intrusion measurements.

The binary molecular diffusion coefficients for NO and NH_3 in N_2 were calculated by the formula of Fuller et al. ([39]). The molecular diffusion coefficient of elemental mercury was described by adopting the correlation proposed by Massman ([40]), valid in the temperature range 0–350 °C and herein extrapolated up to 400 °C:

$$D_{HginN_2} = 0.1211\left(\frac{T}{273.15}\right)^{1.81}(0-350^\circ C)(cm^2/s) \quad (7)$$

For the catalyst tested in this work and at a temperature of 300 °C, we estimate molecular diffusion coefficients of 7.60×10^{-1}, 7.18×10^{-1} and 4.63×10^{-1} cm^2/s and effective diffusion coefficients of 1.91×10^{-2}, 2.37×10^{-2} and 7.92×10^{-3} cm^2/s for NO, NH_3 and Hg° respectively.

3.1.1. Mass balances: $DeNO_X$ process

In the case of the $DeNO_X$ process, the model consists of the mass balances for NO and NH_3 in the gas phase and at the wall; these are reported in Table 1 and closely reproduce the same equations as those discussed in previous studies.

Since the $DeNO_X$ tests herein analysed were performed at high NH_3 concentration, we assumed a simple first order rate expression ($R_{DeNOx} = k_{DeNOx}C_{NO}$). Indeed, we verified that the incorporation of an Eley-Rideal rate expression ($R_{DeNOx} = k_{DeNOx}C_{NO}\theta_{NH3}$) based on an estimate of the NH_3 adsorption constant from independent studies [41], did not affect either the estimate of the intrinsic rate parameter k_{DeNOx}, either the model response. In fact, under the conditions of the experiments the coverage of NH_3 was always unitary.

The role of intraporous mass transfer limitations was accounted for by the incorporation of an efficiency factor, calculated for indefinite slab geometry.

This system of equations provides a complete characterization of the process in terms of axial evolution of the concentration of reactants in the bulk phase and at the bulk-solid interface, provided that the geometrical data, the effective molecular diffusivity and the kinetic parameters for the $DeNO_X$ reaction are known. Model fit to integral data of conversion can be adopted instead to obtain an estimation of the intrinsic rate parameters.

3.1.2. Mass balances: Hg° oxidation process

In the case of Hg° oxidation, the model consists of the single mass balance for Hg°. This is reported in Table 2.

In analogy with the $DeNO_X$ model and in line with Niksa and Fujiwara [19] and Niksa and Sibley [42] approaches, a lumped form was adopted to describe the mass balance of Hg° in the gas phase, Eqs. (20)–(22). The effect of diffusion limitations were taken into account assuming a pseudo first-order effectiveness factor (Eq. (22)).

The form of the rate expression is discussed in the following, based on the experimental evidence herein collected.

As above illustrated, once defined the rate expression, the integration of Eqs. (17)–(23) yields the axial concentration profile of Hg° in the bulk and at the wall, as well as an estimate of the catalyst effectiveness factor, using as input parameters the geometrical data and the kinetic parameters of the rate function; conversely, by adapting the model response to experimental data, an estimate of the kinetic parameters can be obtained. The latter is the approach herein adopted, so that the model was used to analyze quantitatively the reactor response and "extract" intrinsic kinetics from the tests performed in the multichannel reactor cell, which in principle are expected to be affected by both external and internal mass transfer limitations.

3.2. Thermodynamic analysis of Hg° oxidation

Madsen et al. [26,27] have recently shown, by running experiments over a V-based catalyst at low space velocity and comparing them with thermochemical equilibrium calculations, that the oxy-chlorination of Hg° (1) is a reversible process and the thermodynamics are such that Hg° is the favored species at high temperatures. Thus, the thermodynamics of Hg° speciation under the operating conditions herein tested was analyzed in order to verify the possible approach to chemical equilibrium. Fig. 3 shows the calculated mercury conversion at thermodynamic equilibrium under the flue gas conditions of the experiments, at varying HCl inlet concentrations (2, 10, 50 ppm). Equilibrium compositions were calculated by minimizing the Gibbs free energy of the reacting system and using thermochemical data from the NIST database [43].

Fig. 3 shows that at the thermodynamic equilibrium Hg° conversion significantly decreases at decreasing HCl concentration from 50 to 10 to 2 ppm.

However, in this work, the experiments were performed in between 200 and 400 °C. The temperature range is such that at sufficiently high HCl concentration (≥10 ppm), Hg^{2+} is the

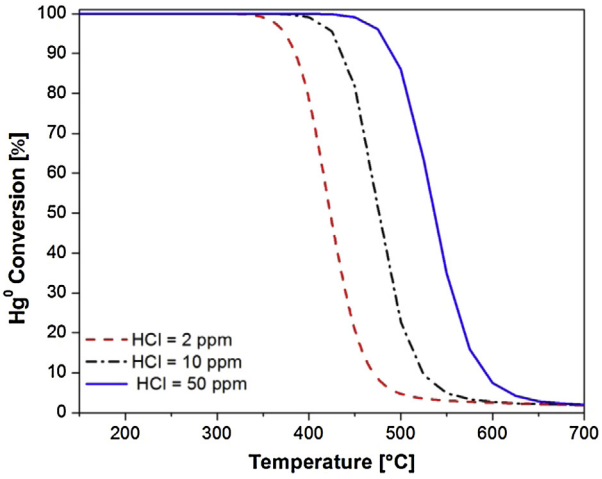

Fig. 3. Thermodynamic analysis. Calculated elemental mercury conversion at the thermodynamic equilibrium varying HCl inlet concentration. Feed composition: Hg° = 10 μg/Nm³; HCl = 2, 10, 50 ppm; H_2O = 10.5%; O_2 = 3.5%; N_2 at balance.

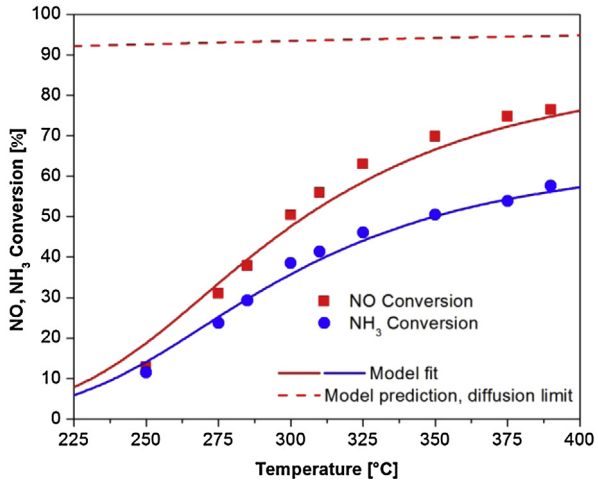

Fig. 4. NH_3-SCR tests. Symbols: experimental NO conversion (squares) and NH_3 conversion (circles). Lines: model fit. Feed composition: NO = 300 ppm; NH_3 = 405 ppm; H_2O = 10.5%; O_2 = 3.5%; N_2 at balance. AV = 21 Nm/h.

thermodynamically favored species. Only at 2 ppm HCl, the analysis predicts an equilibrium conversion of Hg° of about 80% at 400 °C. Thus, in principle, a driving force for the backward reaction may exist under these extreme conditions.

3.3. NH_3-SCR tests and reactor performance

NH_3-SCR tests were performed without feeding mercury or HCl. As mentioned above these tests were performed to characterize on one side the reactivity of the catalyst, on the other side the performance of the reactor, in particular the impact of inter-phase and intraporous mass transfer limitations on the observed conversions.

Fig. 4 (symbols) illustrates the results of the experiments in terms of NO conversion and NH_3 conversion in the temperature range from 250 °C to 400 °C.

It was observed that NO conversion increased in the whole temperature range investigated from 13% at 250 °C to about 76% at 390 °C. NH_3 conversion followed the stoichiometry of the standard SCR reaction ($NO + NH_3 + 1/4O_2 \rightarrow N_2 + 3/2H_2$), with a molar consumption ratio ($= NH_{3converted}/NO_{converted}$) always very close to 1. This suggests that NH_3 oxidation did not occur in the experimental conditions investigated.

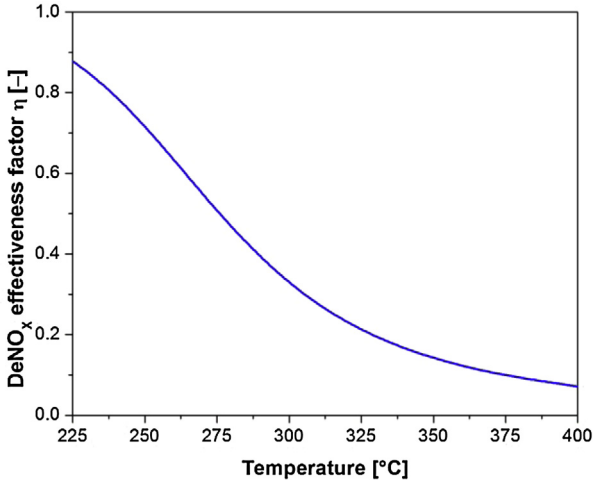

Fig. 5. NH_3-SCR tests. $DeNO_X$ effectiveness factor (η) over temperature.

The reactor model was adapted to the data; the following estimate of the intrinsic rate was obtained,

$$k_{DeNO_X} = \left(7.30 \cdot 10^2\right) exp\left(-\frac{26000}{1.987}\left(\frac{1}{T} - \frac{1}{573.15}\right)\right) (1/s) \qquad (24)$$

and the model predictions are reported in Fig. 4 in solid lines.

The parameter estimate Eq. (24) well compares with the rate constants estimated in a previous kinetic study of SCR over vanadia based commercial catalysts [10].

The impact of intraporous mass transfer limitations was verified by evaluating the effectiveness factor of the slabs. Fig. 5 plots this parameter for one of the inner channels as a function of temperature.

It is observed that the effectiveness factor was significantly below 1 under the whole temperature range investigated: it amounted to about 70% at 250 °C but it dropped down to 15% at 350 °C.

Concerning the role of gas solid mass transfer, the limiting case of fully diffusion controlled regime was simulated by imposing a kinetic constant→ ∞. The predicted conversion thresholds for NO and NH_3 are also reported in Fig. 4 in dashed lines. Notably, the comparison between experimental data and model predictions shows that the NH_3-SCR process was not operating under full mass transfer control, particularly at low temperature, but more properly in a mixed chemical/intraporous diffusion regime.

3.4. Hg° oxidation tests

Reference tests were performed in the absence of the $DeNO_X$ reactants in the temperature range from 170 °C to 400 °C and AV of 21 Nm/h. The inlet mixture composition was: 10 μg/Nm³ Hg°, 50 ppm HCl, 3.5% O_2, 10.5% H_2O and N_2 as carrier gas. Fig. 6 reports the measured conversions.

Two main observations can be done from the data. Firstly, we note that the values of mercury conversion were comparable with the values of NO conversion in the SCR tests. It can be deduced that the two processes have comparable Damköhler numbers (rate of reactions/rate of diffusion) and in turn a similar influence from inter-phase mass transfer limitations. In other words, we can expect that the Hg° conversion measurements were largely controlled by the chemical process in the slabs (limited by intraporous mass transfer) but not fully limited by external mass transfer.

Secondly, the data give a clear evidence of positive temperature dependence over the whole temperature range investigated. Conversion increased from about 20% at 175 °C to about 70% at 400 °C, which corresponds to a an estimate of the apparent

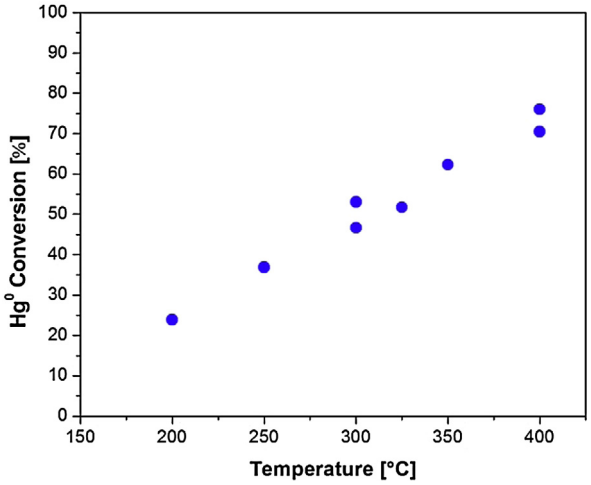

Fig. 6. Hg oxidation tests. Elemental mercury conversion over temperature. Feed composition: Hg° = 50 μg/Nm^3; HCl = 50 ppm; H_2O = 10.5%; O_2 = 3.5%; N_2 at balance; AV = 21 Nm/h.

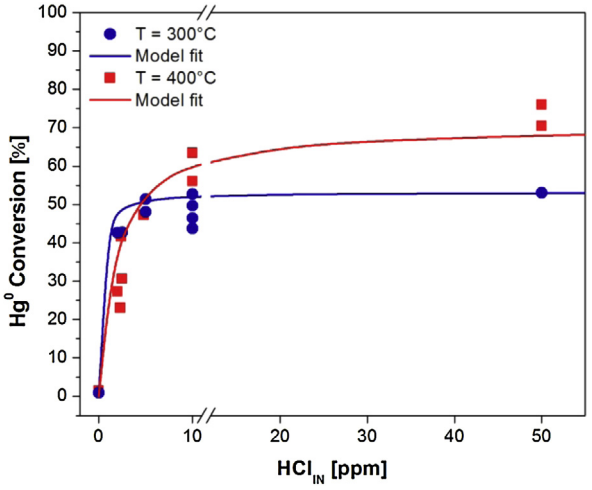

Fig. 7. Hg oxidation tests. Symbols: elemental mercury conversion in the reactor versus HCl inlet concentration. Lines: model fit. Feed composition: Hg° = 10 μg/Nm^3; H_2O = 10.5%; O_2 = 3.5%; N_2 at balance; AV = 21 Nm/h; T = 300 °C (circles), T = 400 °C (squares).

activation energy (under the conventional assumption of pseudo-homogeneous reactor and first order reaction order) of about 4.5 kcal/mole. Considering the mentioned expected impact of intra-porous mass transfer limitations, this well compares with the value of 9 kcal/mole estimated over powders (thus under chemically controlled regime) and DeNO$_X$ inactive conditions (similarly to the present study) by Hocquel and Negreira [44] and Negreira and Wilcox [25].

Conversely, as mentioned in the Introduction, several authors have found the existence of a maximum in the conversion curve, typically in the presence of NH_3. For example, Richardson et al. [45] showed a decrease of mercury oxidation after reaching a maximum at 315 °C. A qualitative similar behaviour was obtained by Senior [21], with a maximum in the Hg oxidation observed at 350 °C.

3.5. Effect of HCl

Experiments on the effect of HCl were carried out with an inlet mixture composition of 10 μg/Nm^3 Hg°, 3.5% O_2, 10.5% H_2O and N_2 as carrier gas. HCl concentration was randomly varied in the range 0–50 ppm. Fig. 7 illustrates the results obtained at 300 and 400 °C.

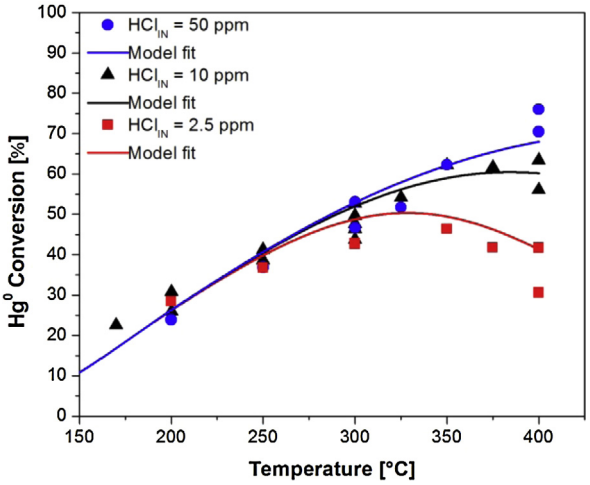

Fig. 8. Hg° oxidation tests. Symbols: combined HCl and temperature effect, Hg° conversion data over temperature. Lines: model fit. Feed composition: Hg° = 10 μg/Nm^3; HCl = 2.5 ppm (squares—10 ppm (triangles)—50 ppm (circles); H_2O = 10.5%; O_2 = 3.5%; N_2 at balance; AV = 21 Nm/h.

At 300 °C, with decreasing HCl concentration, the Hg° conversion (paired by the production of oxidized mercury) kept almost constant down to 5 ppm HCl. Only at lower HCl concentration (2 ppm) a certain drop of conversion was observed. In the absence of HCl, no production of oxidized mercury was observed in the outlet stream; the dynamics of Hg° adsorption were observed under this condition, and the accumulation of mercury extinguished after several hours.

At 400 °C, the qualitative effect of HCl was similar, but a greater sensitivity of the mercury conversion upon a change of HCl concentration was observed. In fact, a net decrease of conversion was observed with HCl content below 10 ppm.

It is interesting to note that the comparison between the two sets of data shows that the temperature dependence changed at varying HCl concentration. In particular, the data showed a negative temperature dependence at the lowest HCl content investigated. Given the importance of this evidence, the effect of HCl on the temperature dependence of the conversion process was further investigated.

3.6. Combined effect of temperature and HCl

Similarly to the tests reported in Fig. 2, Hg° oxidation tests were performed at 2.5 and 10 ppm of HCl at increasing temperature from 200 and 400 °C. Except for the HCl content, the total flow rate and gas composition of the inlet feed were the same as in the reference tests; Fig. 8 compares the results of the three sets of data.

It was found that, at temperature lower than 300 °C, Hg° conversion was insensitive to HCl inlet concentration. For example, at 250 °C, we observed 37% of elemental mercury conversion feeding 2.5 ppm of HCl, 41% feeding 10 ppm HCl and 37% feeding 50 ppm of HCl. The data thus suggest that, in these conditions, HCl was not kinetically limiting; this can be explained by assuming that HCl adsorption on the catalyst surface reached the saturation and all the vanadium sites involved in the reaction were chlorinated.

Instead, at increasing temperature above 300 °C, the conversion of elemental mercury was strongly affected by HCl concentration. While at 50 ppm HCl Hg° conversion progressively grew with temperature, at 10 ppm HCl Hg° conversion tended to flatten at the highest temperatures. Remarkably, at 2.5 ppm HCl, the conversion of elemental mercury passed through a maximum and showed at the highest temperatures a negative trend with increasing

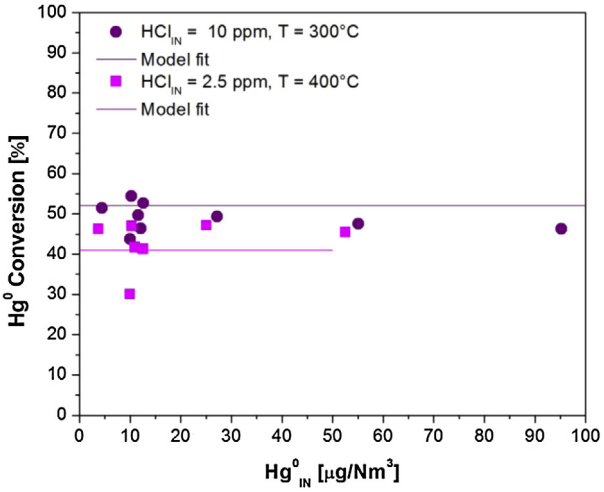

Fig. 9. Hg oxidation tests. Symbols: elemental mercury conversion in the reactor versus Hg° inlet concentration. Lines: Model fit. Feed composition: Hg° = 5–100 μg/Nm^3; HCl = 2.5 ppm (squares)—10 ppm (circles); H_2O = 10.5%; O_2 = 3.5%; N_2 at balance; AV = 21 Nm/h; T = 300–400 °C.

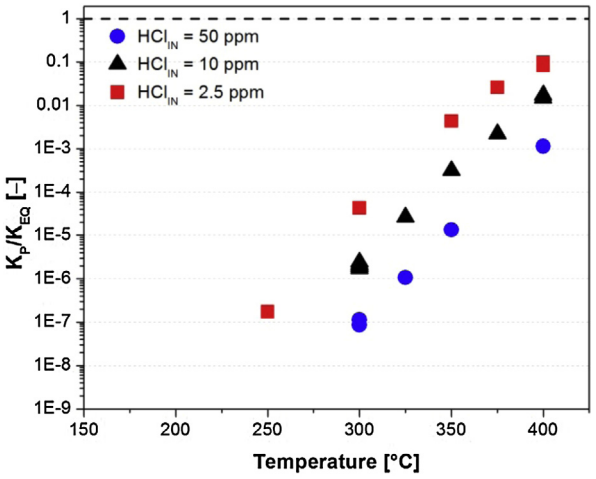

Fig. 10. analysis. Hg° oxidation tests, K_p/K_{eq} calculated ratio (symbols) over temperature. Feed composition: Hg° = 10 μg/Nm^3; HCl = 2.5 ppm (squares)—10 ppm (triangles)—50 ppm (circles); H_2O = 10.5%; O_2 = 3.5%; N_2 at balance; AV = 21 Nm/h.

temperature, with 46% of measured conversion at 350 °C and 29% conversion at 400 °C.

Thus, the data show that above 300 °C, Hg° oxidation was kinetically limited by HCl activation. The observed trends are in line with the effects of temperature and gas phase concentration on the concentration of an adsorbed intermediate. The coverage of a surface species is in fact expected to decrease at increasing temperature and decreasing gas phase concentration.

3.7. Hg° effect

Several studies [10,16] have reported that the efficiency of Hg° oxidation is independent from the gas phase concentration of mercury in the reacting mixture. We investigated this effect by running tests at varying Hg° inlet concentration from 5 to 100 μg/Nm^3. Two sets of experiments were run under the two chemical regimes previously identified: in one case the effect of Hg° concentration was explored under conditions of "insensitivity" of the process from HCl and probable surface saturation (300 °C, 10 ppm HCl), in the other case the effect of Hg° was investigated under a condition of kinetic relevance of HCl content and probable surface depletion of HCl (400 °C, 2.5 ppm HCl). The results are plotted in Fig. 9 (circles vs squares).

At 300 °C, the degree of Hg° conversion was almost insensitive to the change of the Hg° inlet concentration in the wide explored range. For example, elemental mercury conversion was 52% at 5 μg/Nm^3, 49.4% at 27.5 μg/Nm^3 and 46.5% at 95 μg/Nm^3.

At 400 °C and 2.5 ppm HCl, Hg° conversion showed a similar flat trend; the measured conversion amounted to 46% at 5 μg/Nm^3 Hg°, 47 at 25 μg/Nm^3 and 45.4 at 50 μg/Nm^3.

Thus, in both cases, the rate of Hg° oxidation revealed a first order dependence on the gas phase concentration of mercury.

Combined with the data on the effect of HCl, these data allow to better identify the probable reaction pathway and discriminate between the alternative hypotheses that chlorination is or is not limited by mercury activation. The observed trends are in line with the picture of Hg° reacting with chlorinated sites or in general terms [VO_X—HCl] species through a weak adsorption (similarly to NO in the DeNO_X-SCR process). They also show that the chlorination process is not affected by the Hg° concentration, which seems to exclude that chlorination occurred as a consecutive step to the formation of [VO_X—Hg] species. The latter scenario in fact would have been consistent with a negative effect of Hg° concentration on mercury conversion at 400 °C and 2.5 ppm HCl, where the process is kinetically limited by HCl activation.

In other words, based on the present data, the "surface capacity" of chlorine species appears independent from the concentration of mercury.

3.8. Thermodynamic analysis

Before addressing the modelling analysis, we first verified the potential impact of the thermodynamics of mercury speciation on the conversion measurements. The approach to equilibrium in the various experiments was estimated by evaluating the ratio K_p/K_{eq}, where K_{eq} is the equilibrium constant and K_p is the reaction quotient, defined as:

$$K = \left(p_{HgCl_2} p_{H_2O}\right) / \left(p_{Hg^0} p_{HCl}^2 p_{O_2}^{0.5}\right) \quad (25)$$

where p_i is the partial pressure of the i^{th} species.

Fig. 10 shows the calculated ratio K_p/K_{eq} over temperature in the case of 2, 10 and 50 ppm HCl.

We found that K_p/K_{eq} grew with increasing temperature in each set of experiments, but it was always well below the unity except for the case of the experiment at 400 °C and 2.5 ppm HCl. Here, the approach to equilibrium measured by the ratio K_p/K_{eq} was~0.1.

Considering that the presence of a maximum in the conversion curve at 2.5 ppm was centred around 300–350 °C, thus far from equilibrium, we concluded that the observed trends and in particular the negative temperature dependence at 2.5 ppm HCl were not due to the reversibility of the reaction and, on the opposite, the collected data were informative of the kinetics of the forward reaction rate.

3.9. Hg° oxidation kinetics

The experimental results highlight the kinetic dependences:

- at temperature lower than 300 °C, Hg° conversion was insensitive to the HCl inlet concentration; the same tendency was observed at higher temperatures, at sufficiently high HCl concentration. This suggests that HCl reacts as an adsorbed species (whose coverage is close to the catalyst surface capacity under these conditions), and not from the gas phase.
- at high HCl concentration, the observed T-dependence of mercury oxidation was positive; at temperatures higher than 300 °C, the

observed T-trend changed with the HCl content and was negative in the case of 2.5 ppm HCl. This is coherent with the assumption that HCl reacts from the surface; it implies in fact that the overall T-dependence of the process is the result of the combination of the opposed contributions from the reaction steps (positive T-dependence) and the adsorption steps (negative T-dependence).
- at varying temperature and HCl inlet concentration, elemental mercury conversion was insensitive to Hg° inlet concentration; this suggests a first order kinetic dependence on mercury inlet concentration and, as above observed, that the surface capacity of chlorination is an intrinsic property of the catalyst, independent from the mercury concentration.
- Hg° conversion was kinetically, but not thermodynamically, controlled: thus, the contribution of the reverse reaction was negligible.

Thus, the rate expression needs to account for both the dependence on gas phase Hg° concentration and the surface coverage of HCl.

Recent theoretical studies by Zhang et al. [22] and Negreira and Wilcox [23] have identified the most stable intermediates and probable reaction pathway; both thermodynamic and kinetic calculations suggest that the reaction first involves the formation of a chlorinated vanadyl species ($V = O\,[HCl]$), which reacts with gas-phase or weakly adsorbed elemental mercury (similarly to an Eley-Rideal mechanism) to form a surface HgCl intermediate ($V = OH\,[HgCl]$); mercury chloride ($HgCl_2$) is then formed by the consecutive reaction with a second adjacent chlorinated site. Finally, $HgCl_2$ desorbs and the catalytic sites is re-oxidized by gaseous O_2.

The elementary reaction steps of the redox cycle and the corresponding rate expressions can be formalized through a classical approach:

$$\text{Step 1}: S_1 = O + HCl \leftrightarrow S_1 = O[HCl] \tag{26}$$

$$\text{Step2}: Hg^0 + S_1 = O\,[HCl] \leftrightarrow S_1 = OH\,[HgCl] \tag{27}$$

$$\text{Step 3}: S_1 = OH\,[HgCl] + S_1 = O\,[HCl] \rightarrow HgCl_2 + 2S_1 - OH \tag{28}$$

$$\text{Step 4}: 2S_1 - OH + \frac{1}{2}O_2 \rightarrow 2S_1 = O + H_2O \tag{29}$$

where the concentration of redox sites is indicated by S_1, and oxidized $S_1 = 0$ sites are distinguished by reduced $S_1 - OH$ sites in analogy with the same nomenclature introduced by Tronconi et al. [46]. Although not explicitly taken into account, the scheme is not in contrast with the possibility that mercury adsorption and accumulation may occur on the catalyst as clearly observed in several previous studies [11]. Steps 1–4 aim at providing a description of the steady-state kinetic behaviour, that was experimentally analysed in this study.

Step 1 accounts for a generic step of activation of HCl over a $S_1 = 0$ site. Step 2 is the reaction between surface HCl and gas-phase or weakly adsorbed elemental mercury, leading to the formation of an HgCl adsorbed species. This further reacts (Step 3) with an adjacent $S_1 = O\,[HCl]$ site with the formation and desorption of oxidized mercury ($HgCl_2$) and the reduction of the site ($S_1 - OH$). Finally, the catalytic sites are re-oxidized to the original form by gaseous O_2 (Step 4).

If we assume that Step 3 is much slower that Step 1 and Step 2, thus representing the rate determining step, than we can assume that Step 1 and Step 2 will be equilibrated.

Additionally, although the intrinsic rate of re-oxidation of vanadium is expected to be very high, under stationary conditions the rate of site reduction (Step 3) will be equal to the rate of re-oxidation (Step 4), being the latter globally limited by the concentration of reduced sites.

Thus:

$$r_1 = k_1 P_{HCl}\sigma_{ox} - k_{-1}\sigma_{HCl} = 0 \tag{30}$$

$$r_2 = k_2 P_{Hg^0}\sigma_{HCl} - k_{-2}\sigma_{HgCl} = 0 \tag{31}$$

$$r_3 = k_3\sigma_{HgCl}\sigma_{HCl} \tag{32}$$

$$r_4 = k_4 (P_{O_2})^{\frac{1}{2}} (\sigma_{red})^2 \tag{33}$$

From equilibria (30) and (31) we can express σ_{HgCl} and σ_{HCl} as functions of σ_{ox} (the fraction of free oxidized sites):

$$\sigma_{HCl} = K_1 P_{HCl}\sigma_{ox} \tag{34}$$

with $K_1 = k_1/k_1^*$.

$$\sigma_{HgCl} = K_2 P_{Hg^0}\sigma_{HCl} = K_1 K_2 P_{Hg^0} P_{HCl}\sigma_{ox} \tag{35}$$

where $K_2 = k_2/k_2^*$.

By replacing σ_{HgCl} in Eq. (32), we derive:

$$r_3 = k_3 K_2 P_{Hg^0}(\sigma_{HCl})^2 = k_3 K_2 P_{Hg^0}(K_1 P_{HCl}\sigma_{ox})^2 \tag{36}$$

Imposing that the rate of Step 3 be equal to the rate of Step 4, we obtain the following relationship between chlorinated and reduced sites:

$$\sigma_{red} = \sigma_{HCl}\left(\frac{k_3 K_2 P_{Hg^0}}{k_4 \left(P_{O_2}\right)^{1/2}}\right)^{1/2} \tag{37}$$

and between reduced and oxidized sites:

$$\sigma_{red} = \left(\frac{k_3 K_2 P_{Hg^0}}{k_4 \left(P_{O_2}\right)^{\frac{1}{2}}}\right)^{\frac{1}{2}} K_1 P_{HCl}\sigma_{ox} \tag{38}$$

Considering now the overall site balance:

$$1 = \sigma_{ox} + \sigma_{HCl} + \sigma_{HgCl} + \sigma_{red} \tag{39}$$

And expressing $\sigma_{HCl}, \sigma_{HgCl}$ and σ_{red} as function of σ_{ox}, we obtain a condition for σ_{ox}. In fact:

$$1 = \sigma_{ox} + K_1 P_{HCl}\sigma_{ox} + K_1 K_2 P_{Hg^0} P_{HCl}\sigma_{ox} + \left(\frac{k_3 K_2 P_{Hg^0}}{k_4 \left(P_{O_2}\right)^{\frac{1}{2}}}\right)^{\frac{1}{2}} K_1 P_{HCl}\sigma_{ox} \tag{40}$$

The four terms in left hand side of Eq. (40) have very different orders of magnitude; we can in fact expect that being P_{Hg^0} close to zero ($P_{Hg^0} \ll P_{HCl}$), the third term (σ_{HgCl})will be negligible with respect to the second one (σ_{HCl}). Also, the term $k_3 P_{Hg^0}/k_4 \left(P_{O_2}\right)^{\frac{1}{2}}$ is expected to be close to zero since P_{Hg^0} is negligible compared to P_{O2} and the intrinsic rate of re-oxidation is expected to be very high (so that $\frac{k_3}{k_4} \ll 1$). Thus, the site balance Eq. (40) reduces to the following simple condition:

$$1 = \sigma_{ox} + K_1 P_{HCl}\sigma_{ox} \tag{41}$$

from which:

$$\sigma_{ox} = \frac{1}{1 + K_1 P_{HCl}} \tag{42}$$

Combining Eq. (42) with Eq. (36), we obtain the following:

$$r_{Hg} = r_3 = r_4 = k_{Hg} P_{Hg^0}\left(\frac{K_1 P_{HCl}}{1 + K_1 P_{HCl}}\right)^2 \tag{43}$$

where $k_{Hg} = k_3 K_2$.

The proposed reaction scheme is coherent with several theoretical and experimental findings concerning the formation of chlorinated V-sites [19,20,22], the intermediate formation of HgCl [22,23] and the weak adsorption of $HgCl_2$ [22,23]. The added value is the formalization of the kinetic dependences, including the

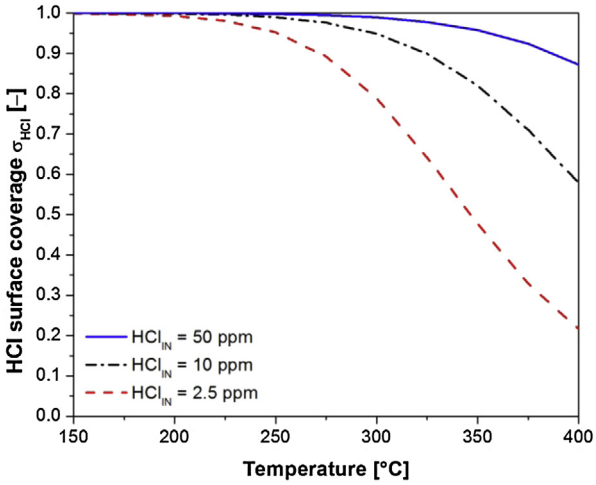

Fig. 11. HCl surface coverage (σ_{HCl}) over temperature at varying HCl inlet concentration. Operating conditions as in Fig. 8.

dependence from the gas phase HCl concentration and, very important, the dependence on temperature. This relies on one side on the T-dependence of $k_{Hg} = k_3K_2$ (thus the combined effect of the intrinsic activation energy of Step 3 and the reaction enthalpy of Step 2) and on the other side on the T-dependence of the group $(\sigma_{HCl})^2$ which depends on the enthalpy of Step 1.

The rate expression (43) has been incorporated in the model and adapted to the bulk of data, adopting the following modified temperature functions, "centred" on a reference temperature T_{ref}:

$$k_{Hg} = k_{Hg}\left(T_{ref}\right) exp\left(-\frac{E_{act}}{R}\left(\frac{1}{T}-\frac{1}{T_{ref}}\right)\right) \quad (44)$$

$$K_1 = K_{HCl} = K_{HCl}\left(T_{ref}\right) exp\left(-\Delta H_{HCl}/R\left(\frac{1}{T}-\frac{1}{T_{ref}}\right)\right) \quad (45)$$

Pre-exponential factors and energy parameters were estimated as follows:

$$k_{Hg} = \left(8.80\cdot 10^{1}\right) exp\left(-\frac{14000}{1.987}\left(\frac{1}{T}-\frac{1}{573.15}\right)\right)(1/s) \quad (46)$$

$$K_{HCl} = \left(4.46\cdot 10^{8}\right) exp\left(\frac{20000}{1.987}\left(\frac{1}{T}-\frac{1}{573.15}\right)\right)\left(cm^3/mol\right) \quad (47)$$

The model fit is shown in Figs. 7–9 in solid lines and was very satisfactory. The proposed kinetic expression and the reactor model allow to describe with good accuracy the observed effects. Namely, the model is able to correctly describe the insensitivity of Hg° conversion to HCl inlet concentration at temperatures lower than 300 °C, the modulated temperature dependence at varying HCl concentration from 50 to10 to 2.5 ppm with the presence of a broad maximum of Hg° conversion at the lowest HCl content. Furthermore, it can be noted from Figs. 7 and 9 that the model well explained the experimental trends observed in mercury oxidation tests performed at varying HCl and Hg° inlet concentration.

The "explanation" behind the combined temperature-HCl effect is giver by Fig. 11, which plots the calculated trend of HCl surface coverage (σ_{HCl}) under the experimental conditions reported in Figs. 7 and 8 (varying temperature and HCl inlet concentration of 2, 10 and 50 ppm).

HCl surface coverage was close to 1 (>0.95) at the lowest temperatures investigated (below 250 °C) at any HCl concentration. As result, Hg° conversion becomes insensitive to HCl feed content. At increasing temperature up to 400 °C, the calculated HCl surface coverage moderately decreases to 0.85 at 50 ppm HCl, it decline to 0.55 at 10 ppm HCl and it drastically drops to 0.23 in the case of 2.5 ppm HCl. These differences explain the temperature dependence showed by experimental data: feeding 50 ppm of HCl, Hg° conversion increased almost linearly with temperature due to the fact that HCl surface coverage was in the whole set close to unity. At 10 ppm HCl, elemental mercury conversion progressively increased with temperature up to 350 °C (where σ_{HCl} was higher than 0.8) and then tended to flattering from 350 °C to 400 °C: in this conditions, the positive effect of temperature on the reaction is balanced by the lack of adsorbed HCl. This effect was more emphasized at 2.5 ppm of HCl: at temperature higher than 300 °C, HCl surface coverage dropped drastically and the conversion suffered more severely this surface depletion.

3.10. Comments on the energy parameters

The combined T-HCl effects are well described by assuming a high value of the heat of reaction for Step 1 ($\Delta H_{HCl} = -20$ Kcal/mol in Eq. (47)). This may be in contrast with the expected heat of an adsorption step, while it is coherent with the energetics of a reaction step (that is the chlorination of vanadia sites). Indeed, Navarro et al. [47] have recently studied the thermodynamics of the carbon-chlorination of V_2O_5 and proposed several stoichiometries for the chlorination of several V-species. Based on the thermochemical data provided by their study, we analysed the thermodynamics of V_2O_5 chlorination; it was found that the most stable chlorinated form of vanadium oxides is the VO_2Cl species, although its expected concentration at equilibrium rapidly decreases with temperature ad is extremely low under the experimental conditions investigated in this work (150–400 °C). This suggests a possible stoichiometry for Step 1, that is:

$$V_2O_5 + 2HCl \leftrightarrow 2VO_2Cl + H_2O \quad (48)$$

whose heat of reaction is estimated at about −15 kcal/mol. We believe that this value provides a reasonable confirmation of the physico-chemical consistency of the estimated heat of reaction herein found for Step 1 (−20 Kcal/mol), considering that the thermodynamic calculations refer to the ideal case of pure bulk solids and that a variety of chlorination stoichiometries exist with widely varying heats of reactions (15 ÷ −24 Kcal/mole).

Concerning the activation energy, a relatively low value is found (14 kcal/mole); however, by remembering that this is a "global" energy term accounting also for the exothermic formation of the HgCl surface intermediate (estimated at about −12.4 Kcal/mole by Zhang et al. [22]) then the expected intrinsic energy barrier of the elementary Step 3 is higher than 14 kcal/mole.

As a final comment, we note that most of the results and assumptions of this work are in line with the DFT study by Zhang et al. [22]; however these authors proposed two possible reaction pathways in which pathway 1 passes through the reaction of a surface HgCl intermediate with gas-phase HCl, while pathway 2 accounts for the reaction of the HgCl intermediate with an adjacently activated HCl species. The experimental evidence herein provided and the kinetic scheme herein developed are in favour of pathway 2, since it uniquely explains the surface saturation effect by HCl, that is the disappearance of a kinetic dependence form the gas-phase concentration of HCl under certain operating conditions. Pathway 1 would instead imply a residual kinetic dependence of the reaction rate from the HCl feed content. Our kinetic treatment is also very close to the proposal and quantitative results by Negreira and Wilcox [23].

3.11. Analysis of the reactor cell performance

The model herein developed represents a useful tool for the analysis of the reactor performance; in particular, it is possible to evaluate the influence of both external and internal mass transfer

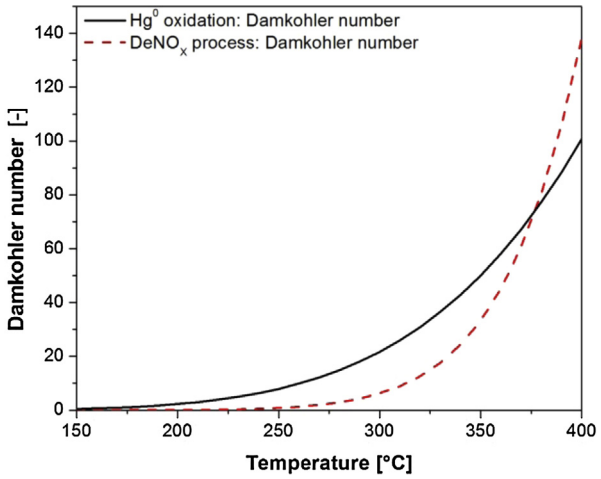

Fig. 12. Calculated Damköhler numbers of $DeNO_X$ process (Da_{DeNOx}) and Hg° oxidation (Da_{Hg}) over temperature.

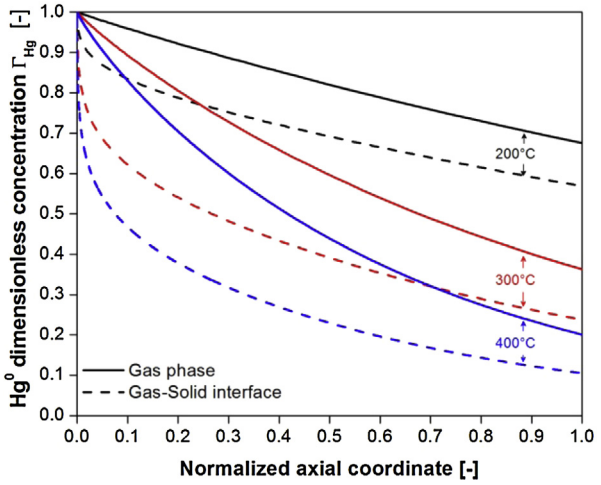

Fig. 13. Calculated profiles of the Hg° dimensionless concentration (Γ_{Hg}) along the reactor (inner channel) at different temperatures. Solid lines: Gas phase concentration. Dashed lines: Gas-Solid interface concentration. Feed composition: Hg° = 10 μg/Nm³; HCl = 50 ppm; H_2O = 10.5%; O_2 = 3.5%; N_2 at balance; AV = 21 Nm/h; T = 200–300–400 °C.

limitations on elemental mercury conversion under the experimental conditions investigated.

Concerning the role of external mass transfer limitations, Fig. 12 shows the calculated value of the Damköhler number for Hg° oxidation (Da_{Hg}) over temperature; this is compared for reference with the calculated Damköhler number for $DeNO_X$ process (Da_{DeNOx}).

As above discussed (Fig. 4, diffusion limit), at low temperature the effect of external mass transfer limitations on $DeNO_X$ process is negligible: in fact, Da_{DeNOx} is lower than 1 in the range below 250 °C and lower than 10 for temperature below 300 °C. In these conditions, the process is operating under a mixed chemical/internal diffusion regime. Gas-solid mass transfer becomes more relevant only at temperatures higher than 350 °C where $Da_{DeNOx} > 30$.

In the case of Hg° oxidation, as expected from the conversion levels, the values of Da_{Hg} are comparable to the values of Da_{DeNOx} with a maximum value of about 100 at 400 °C. It is thus confirmed that, under the operating conditions explored in this work, the reactor cell operated under a mixed regime greatly controlled by the kinetic process at the wall. To better highlight the effect of gas-solid diffusion Fig. 13 plots the calculated axial concentration profiles of elemental mercury in the bulk phase and at the wall

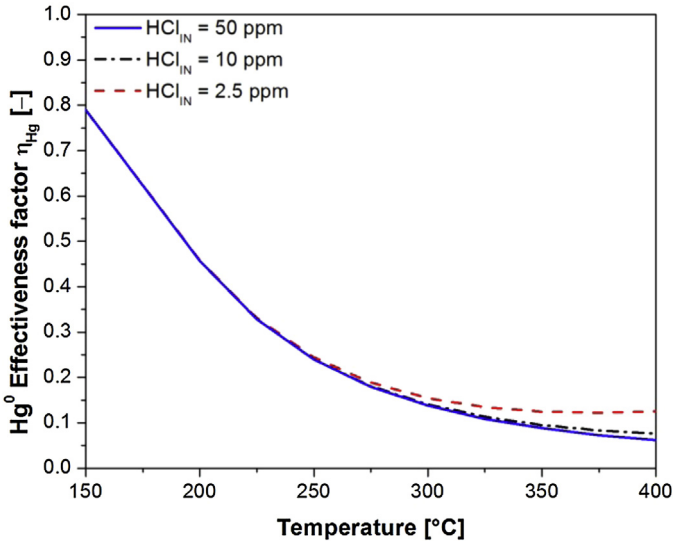

Fig. 14. Hg° effectiveness factor (η_{Hg}) over temperature.

for three characteristic temperatures. Indeed, at increasing temperature from 200 to 300 to 400 °C, the intensity of the interphase gradient becomes more important but the reactor operated far from a full diffusion control; this is fully in line with the results of a previous modelling analysis of pilot scale data over commercial monolith catalysts (Beretta et al. [10]).

Fig. 14 analyses the impact of intraporous diffusion; here the values of the effectiveness factor (η_{Hg}) are estimated according to Eq. (22) in the range between 150 °C and 400 °C, at different HCl inlet concentrations.

As in the case of the $DeNO_X$ process (Fig. 5), the effectiveness factor was found to be significantly lower that unity within the whole range of temperature investigated; in particular we estimate that it amounted to about 45% at 200 °C, 15% at 300 °C and about 10% at 400 °C.

4. Conclusions

In this work, a systematic experimental investigation allowed to give a coherent picture of the main kinetic dependences that the process of Hg° oxidation manifests under the so-called $DeNO_X$ inactive conditions.

The experimental investigation was performed in an integral reactor where the catalyst was tested in the real form (slabs cut from plates); the means of modelling was thus crucial for the analysis of data and the "extraction" of intrinsic kinetics.

The rate expression was derived by assuming a redox cycle wherein a stepwise chlorination sequence ($Hg^\circ \rightarrow HgCl_{ads} \rightarrow HgCl_2$) consumes surface HCl species and reduces the catalytic site, eventually re-oxidized by gas-phase oxygen.

The observed phenomenology of this complex reaction is dominated by the role of surface HCl species (likely chlorinated oxidized V sites). Under the operating conditions of this study, we had evidence that this quantity is thermodynamically and not kinetically controlled, such that it reaches saturation at sufficiently low temperature and/or sufficiently high HCl concentration in the gas-phase. The observed T-dependence of the process is thus influenced not only by the intrinsic activation energy of the surface reaction step, but also by the thermodynamics of HCl coverage, which may determine the negative T-dependences widely reported in the literature and here observed at very low HCl feed content.

An important implication of the kinetic treatment here proposed is that chlorination involves all the redox sites; this opens the question on how this copes with the evidence largely reported in the literature that the presence of HCl does not affect the $DeNO_X$ reactivity. This will be studied in future works also exploiting the means of surface characterization. Further developments of the kinetic investigation will the focus on the effects of the co-presence of NO and/or NH_3, which is also expected to affect the availability of oxidized sites and could thus provide additional pieces of evidence on the adequacy of the reaction scheme proposed.

Acknowledgements

The authors gratefully thank Dr. Dave Thompsett, Dr. Paul Andersen and M.Sc. David Repp from for Johnson Matthey, Technology Center for useful discussion and careful reviewing of the paper.

Bibliography

[1] Y. Gao, Z. Zhang, J. Wu, L. Duan, A. Umar, L. Sun, Z. Guo, Q. Wang, Environ. Sci. Technol. 47 (2013) 10813–10823.
[2] B.M. Reddy, N. Durgasri, T.V. Kumar, S.K. Bhargava, Cat. Rev. Sci. Eng. 54 (2012) 344–398.
[3] EPA, Mercury and air toxics standards (MATS) (2011).
[4] Y.E. Yudovich, M.P. Ketris, Mercury in coal: a review part 2, Int. J. Coal Geol. 62 (2005) 135–165.
[5] T.N. Brown, D.N. Smith, R.A. Hargis Jr, W.J. O'Dowd, J. Air Waste Manage. Assoc. 49 (1999) 628–640.
[6] Y. Tan, R. Mortazavi, B. Dureau, M.A. Douglas, Fuel 83 (2004) 2229–2236.
[7] S.J. Lee, Y.C. Seo, H.N. Jang, K.S. Park, J.I. Baek, H.S. An, K.C. Song, Atmos. Environ. 40 (2006) 2215–2224.
[8] H. Kamata, S.I. Ueno, T. Naito, A. Yukimura, Ind. Eng. Chem. Res. 47 (2008) 8136–8141.
[9] H. Kamata, S.i. Ueno, T. Naito, A. Yamaguchi, S. Ito, Catal. Commun. 9 (2008) 2441–2444.
[10] A. Beretta, N. Usberti, L. Lietti, P. Forzatti, M. Di Blasi, A. Morandi, C. La Marca, Chem. Eng. J. 257 (2014) 170–183.
[11] S. Straube, T. Hahn, H. Koeser, App.Cat. B 79 (2008) 286–295.
[12] H.J. Hong, S.W. Ham, M.H. Kim, S.M. Lee, J.B. Lee, Korean J. Chem. Eng. 27 (2010) 1117–1122.
[13] S. Eswaran, H.G. Stenger, Energy Fuels 19 (2005) 2328–2334.
[14] Y. Zhuang, J. Laumb, R. Liggett, M. Holmes, J. Pavlish, Fuel Process. Technol. 88 (2007) 929–934.
[15] S. Eswaran, H.G. Stenger, Effect of halogens on mercury conversion in SCR catalysts, Fuel Process. Technol. 89 (2008) 1153–1159.
[16] R. Stolle, H. Koeser, H. Gutberlet, App. Cat. B 144 (2013) 486–497.
[17] B.W. Vosteen, R. Kanefke, H. Köser, VGB PowerTech 86 (2006), 70–75 + 76.
[18] S. He, J.S. Zhou, Y.Q. Zhu, Z.Y. Luo, M.J. Ni, K.F. Cen, Zhejiang Daxue Xuebao (Gongxue Ban)/J. Zhejiang Univ. (Eng. Sci.) 44 (2010) 1773–1780.
[19] S. Niksa, N. Fujiwara, J. Air Waste Manage. Assoc. 55 (2005) 1866–1875.
[20] Y. Eom, S.H. Jeon, T.A. Ngo, J. Kim, T.G. Lee, Catal. Lett. 121 (2008) 219–225.
[21] C.L. Senior, J. Air Waste Manage. Assoc. 56 (2006) 23–31.
[22] B. Zhang, J., Liu, G., Dai, M., Chang, C. Zheng, Proceedings of the Combustion Institute (2014).
[23] A. Suarez Negreira, J. Wilcox, J. Phys. Chem. C 117 (2013) 1761–1772.
[24] J. Yang, Q. Yang, J. Sun, Q. Liu, D. Zhao, W. Gao, L. Liu, Cat. Comm. 59 (2014) 78–82.
[25] A.S. Negreira, J. Wilcox, Energy Fuels 29 (2015) 369–376.
[26] J.A.D. Madsen K., Thogersen J.R., Frandsen F., Air Quality VII Conference Arlington (2011).
[27] K. J.A.D. Madsen, J.R. Thogersen, F. Frandsen, Mercury Oxidation over SCR Catalysts for NOx control, ICC 2012 Munich (2012).
[28] F. Frandsen, K. Dam-Johansen, P. Rasmussen, Prog. Energy Combust. Sci. 20 (1994) 115–138.
[29] K.C. Galbreath, C.J. Zygarlicke, Environ. Sci. Technol. 30 (1996) 2421–2426.
[30] T. Nishitani, I. Fukunaga, H. Itoh, T. Nomura, Chemosphere 39 (1999) 1–9.
[31] H. Kamata, S.i. Ueno, N. Sato, T. Naito, Fuel Process. Technol. 90 (2009) 947–951.
[32] H. Kamata, A. Yukimura, Fuel Process. Technol. 104 (2012) 295–299.
[33] H. Li, Y. Li, C.Y. Wu, J. Zhang, Chem. Eng. J. 169 (2011) 186–193.
[34] US EPA Interim Mercury Traceability Protocol (http://www3.epa.gov/ttn/emc/metals.html).
[35] A. Beretta, C. Orsenigo, N. Ferlazzo, E. Tronconi, P. Forzatti, F. Berti, Ind. Eng. Chem. Res. 37 (1998) 2623–2633.
[36] E. Tronconi, P. Forzatti, AIChE J. 38 (1992) 201–210.
[37] G. Groppi, A. Belloli, E. Tronconi, P. Forzatti, Chem. Eng. Sci. 50 (1995) 2705–2715.
[38] N. Wakao, J.M. Smith, Ind. Eng. Chem. Fund. 3 (1964) 123–127.
[39] P.D.S.E.N. Fuller, J.C. Giddings, Ind. Eng. Chem. Res. 58 (1966) 18–27.
[40] W.J. Massman, Atmos. Environ. 33 (1999) 453–457.
[41] N. Usberti, M. Jablonska, M.D. Blasi, P. Forzatti, L. Lietti, A. Beretta, Appl. Catal. B 179 (2015) 185–195.
[42] S. Niksa, A.F. Sibley, Ind. Eng. Chem. Res. 49 (2010) 6332–6341.
[43] NIST Chemistry WebBook, in: NIST (Ed.), 2013.
[44] M. Hocquel, S. Unterberger, K.R.G. Hein, H. Appl, T. König, Dynamisches verhalten von Hg an SCR-DENOX-katalysatoren 83 (2003) 116–119.
[45] C. Richardson, T. Machalek, S. Miller, C. Dene, R. Chang, J. Air Waste Manage. Assoc. 52 (2002) 941–947.
[46] I. Nova, C. Ciardelli, E. Tronconi, D. Chatterjee, B. Bandl-Konrad, AIChE J. 52 (2006) 3222–3233.
[47] E.A. Brocchi, R.C.S. Navarro, F.J. Moura, Thermochim. Acta 559 (2013) 1–16.